INTERIM
IN-92-CR

Structure and Dynamics of Coronal Plasmas

NASA Grant NAGW-4081

Progress Report

For the Period 1 July 1996 through 30 June 1997

Principal Investigator
Dr. Leon Golub

April 1997

Prepared for:

National Aeronautics and Space Administration
Headquarters
Washington, DC 20546

Smithsonian Institution
Astrophysical Observatory
Cambridge, Massachusetts 02138

The Smithsonian Astrophysical Observatory
is a member of the
Harvard-Smithsonian Center for Astrophysics

The NASA Technical Officer for this grant is Dr. William J. Wagner, Code SR, NASA Headquarters, Washington, DC 20546-0001.

corona, and that simple magnetic field extrapolations provide only a poor fit to the observed structure.

A copy of the paper is appended to this report.

II. Plans for the Current Year:

Our plans for continuation of this work during the current year include i) projects which are under development and which are expected to lead to presentations, either in oral or written form, within the year, and ii) completion of the projects described above by submission of papers to refereed journals.

Among the projects which are under development at the present time, we mention the following:

1. "A Converging Flux Model for Point-Like Brightenings Around Sunspots." In collaboration with E. Priest and C. Parnell, we are analyzing coronal, chromospheric and photospheric data of intense x-ray brightenings in Moving Magnetic Features around sunspots. The work includes development of an MHD model for energy release by reconnection, consistent with the observed evolution of the photospheric field, and with the observed coronal energy release parameters.

2. "Coronal Fine Structure." In collaboration with Dr. P. Ulmschneider, we are working on calculations and simulations which will indicate the physical properties of fine structure within coronal loops, related to the coronal heating process. This work is intended to guide future observations by predicting the spatial extent of such fine structure, its location, and the temperatures and densities of the heated regions.

Progress Report

I. Work Completed During the Past Year:

During the past year this grant has funded research in the interaction between magnetic fields and the hot plasma in the solar outer atmosphere. The following is a brief summary of the published papers, abstracts and talks which have been supported by Grant NAGW-4081 within the present grant performance period.

1. The paper "Coronal Structures Observed in X-rays and Hα Structures" was published in the Kofu Symposium proceedings. The study analyzes cool and hot behavior of two x-ray events, a small flare and a surge. We find that a large Hα surge appears in x-rays as a very weak event, while a weak Hα feature corresponds to the brightest x-ray emission on the disk at the time of the observation. Calculations of the heating necessary to produce these signatures, and implications for the driving and heating mechanisms of flares vs. surges are presented.

A copy of the paper is appended to this report.

2. The paper "Differential Magnetic Field Shear in an Active Region" has been published in The Astrophysical Journal. We have compared the 3D extrapolation of magnetic fields with the observed coronal structure in an active region. Based on the fit between observed coronal structure throughout the volume of the region and the calculated magnetic field configurations, we propose a differential magnetic field shear model for this active region. The decreasing field shear in the outer portions of the AR may indicate a continual relaxation of the magnetic field with time, corresponding to a net transport of helicity outward.

A copy of the paper is appended to this report.

3. The paper "Difficulties in Observing Coronal Structure has been accepted for publication in the journal Solar Physics. In this paper we discuss the evidence that the temperature and density structure of the corona are far more complicated than had previously been thought. The discussion is based on five studies carried out by our group on coronal plasma properties, showing that any one x-ray instrument does see all of the plasma present in the corona, that hot and cool material may appear to be co-spatial at a given location in the

DIFFERENTIAL MAGNETIC FIELD SHEAR IN AN ACTIVE REGION

B. SCHMIEDER,[1] P. DÉMOULIN,[1] G. AULANIER,[1] AND L. GOLUB[2]

ABSTRACT

The three-dimensional extrapolation of magnetic field lines from a magnetogram obtained at Kitt Peak allows us to understand the global structure of the NOAA active region 6718, as observed in X-rays with the Normal Incidence X-ray Telescope (NIXT) and in Hα with the Multichannel Subtractive Double Pass spectrograph (MSDP) in Meudon on 1991 July 11. This active region was in a quiet stage. Bright X-ray loops connect plages having field strengths of ~300 G, while Hα fibriles connect penumbrae having strong spot fields to the surrounding network. Small, intense X-ray features in the moat region around a large spot, which could be called X-ray–bright points, are due mainly to the emergence of magnetic flux and merging of these fields with surrounding ones. A set of large-scale, sheared X-ray loops is observed in the central part of the active region. Based on the fit between the observed coronal structure and the field configurations (and assuming a linear force-free field), we propose a *differential magnetic field shear* model for this active region. The decreasing shear in outer portions of the active region may indicate a continual relaxation of the magnetic field to a lower energy state in the progressively older portions of the AR.

Subject headings: MHD — Sun: faculae, plages — Sun: magnetic fields

1. INTRODUCTION

Because of the high conductivity of the coronal plasma along magnetic field lines, and because of the low β of the plasma, the structure in an active region is determined largely by the magnetic field. Observations of the magnetic field in the photosphere is commonly based on the splitting of lines due to the Zeeman effect. At the photospheric level, only the distribution of magnetic flux is measured, while the field topology (field line connectivity) is difficult to establish from the photospheric field measurements. Although some high-resolution microwave interferometry is beginning to be used to deduce the magnetic structure in the corona, it is still necessary to assume a model for both the coronal field and plasma. Alternatively, to infer the large-scale three-dimensional structure at heights above those at which the magnetograph measurements are made (>1000 km) we can extrapolate the measured photospheric field (Alissandrakis 1981; Sakurai 1982; Hannakam, Gary, & Teuber 1984) using a variety of successively more elaborate methods. If any currents in the region are confined to heights at or below the photosphere, the field above is a potential field. If not, a force-free field configuration ($J \times B = 0$, $\nabla \times B = \alpha B$) is commonly assumed because of the low plasma β, corresponding to $J \parallel B$.

This theoretical assumption has recently received support from observations: Metcalf et al. (1995) show, by computation of the magnetic field from the Stokes parameters observed in the Na I line, that the photospheric field is not force free but that it becomes force free roughly 400 km above the photosphere in a quiet active region.

There have been only a limited number of attempts in recent years to carry out direct comparisons between high-resolution coronal observations and magnetic field extrapolations. Several attempts have been made to explain the onset of flares by testing the nonpotentiality of the fields. Typically, $B_\perp$ is compared with Hα fibrils (Schmieder et al. 1990) or Lyα fibrils (Gary et al. 1987). For nonflaring regions, only a few attempts have been made. Poletto et al. (1975), and Sakurai & Uchida (1977) successfully modeled some connected active regions observed with *Skylab* by using potential extrapolations of photospheric fields, and Sams, Golub, & Weiss (1992) confirmed a general agreement by using NIXT observations. Recently, McClymont & Mikic (1994) used a three-dimensional magnetohydrodynamic (MHD) code to analyze a highly sheared region; they found that, in agreement with observations, the highly sheared loops should have a thickness variation along their lengths of only 10%–20%.

It is reasonable to ask whether we always need such a huge code and supercomputer resources to analyze the magnetic fields of active regions. Do less sophisticated methods of extrapolation, which are much faster and more economical, give some insight into the observations? In the present study, we use a linear force-free field extrapolation, discuss its limitations, and show that some significant insights can be gained in understanding the observation. In particular, we may ask how the observed coronal loops correspond to the extrapolated magnetic field lines under this hypothesis and why the connectivity of the X-ray–bright structures follows the topology which is observed.

For this study, we have available a set of high-resolution data sets of a "quiet" active region in Hα obtained with the Meudon MSDP, in soft X-ray observed by NIXT, and magnetic data from Kitt Peak. We have compared extrapolated magnetic field lines above the AR 6718 on 1991 July 11 with cold and hot structures by using Hα fibrils and filaments (MSDP) and X-ray loops (NIXT).

2. INSTRUMENTS

2.1. *NIXT*

The Normal Incidence X-ray Telescope (NIXT) was launched on a NASA sounding rocket 1991 July 11 at 17:25 UT, during a solar eclipse. The NIXT instrument observes

[1] Observatoire de Paris, Section de Meudon, URA 2080, 92195 Meudon, Cedex Principal, France.
[2] Smithsonian Astrophysical Observatory, Harvard-Smithsonian Center for Astrophysics, Cambridge, MA 02138.

problem is discussed self-consistently in order to understand the mechanism which increases the pressure at the surge base (see for more details Schmieder *et al.* 1994b). The basic idea is that if the surge is pressure driven, then the driver gas is expected to be visible in X-rays.

Table 1 Coronal Parameters Measured by the NIXT Instrument.

T_e (10^6 K)	Relative Sensitiv.	Height (10^9 cm)	EI_{min} (10^28 cm^{-5})	EI @ C —	EI @ G —	n_e @ C (10^9 cm^{-3})	n_e @ G —
3.00	1.	15	0.56	3.4	67	1.5	6.6
2.0	0.63	10	0.9	5.4	108	2.4	11
1.5	0.90	7.5	0.6	3.6	72	2.4	11
1.0	4.5	5	0.13	0.82	14	1.2	5.5

If this temperature is well below 10^6 K then the emission from the driver gas would be outside the sensitivity range of NIXT (Table 1). However, there are several arguments against such a low temperature. First, we note that the driving gas must have a temperature of at least 10^5 K in order to raise the plasma to the observed height if there is no injection of cool material from below. In addition, the radiative cooling time for plasma at that temperature is very short compared with the expansion time of the driver gas; consequently there would have to be continuous heating in order to maintain the driver temperature. A continuous heating, however, would inevitably drive the temperature to values well above 10^5 K.

Note that the emission intensity, EI, is strongly dependent on the filling factors . If they are of order unity then the emission measure would be easily observable by NIXT.

3. Conclusion

Hence, our observations rule out the pressure driven models with large filling factors. On the other hand, if the filling factors are of order 10%, then EI is reduced by 4 orders of magnitude, and would not be observable by NIXT. An important question, therefore, is how we can evaluate the filling factors.

References

1. Schmieder, B., Mein N., Golub, L., Davila, J.M., Brosius, J. Thomas, R., 1993, SOHO workshop, ESA SP 348, 257
2. Schmieder, B., Mouradian Z., Golub, L., Antiochos, S.K., 1994a, *Memorie del'Osserv. di Catania*
3. Schmieder, B., Golub, L., Antiochos, S.K., 1994b, *ApJ* in press

the full disk with a resolution less than 1"; it is described in detail by Spiller et al. (1991). The multilayer mirror has a passband of 1.4 Å at 63.5 Å corresponding to two coronal lines, one of Mg x and one of Fe xvi, formed at $T \sim 1 \times 10^6$ K and 3×10^6 K, respectively. The brightening of Mg x occurs near loop footpoints and often coincides with bright chromospheric regions of higher magnetic field strength (network, plages) and of higher density (Peres, Reale, & Golub 1994; Golub, Zirin, & Wang 1994). The brightening is caused by the presence at the loop footpoint of $T \sim 10^6$ K material with sufficient emission measure to produce a visible brightening. This is found to occur typically in the higher pressure coronal loops. Four long-exposure (30 and 60 s) images were obtained between 17:27:11 UT and 17:30:45 UT. For the present study, we use the same notation to identify the main X-ray structures (B, C, E, W) as Golub et al. did.

2.2. MSDP

On July 11 the Multichannel Subtractive Double Pass (MSDP) spectrograph was operating at the Meudon Solar Tower. Its good spatial resolution (1"–1".5) allows us to see the fine chromospheric structures: fibrils and filaments which will be used for coalignment with the extrapolated magnetic field lines. The MSDP provides nine different wavelength channels of the same two-dimensional area of the Sun (Mein 1977). Some details of the data reduction procedures have been presented in Schmieder, Golub, & Antiochos (1994). The data allow us to reconstruct by interpolation a line profile for each pixel in the field of view. For a given chord ($\Delta\lambda$), the intensity is computed in each pixel, and maps of intensities can be displayed. The standard value for $\Delta\lambda$ is taken equal at 0.6 Å, which corresponds commonly to the half-width of the Hα profile at which the contrast of chromospheric fine structures is generally the best.

2.3. Magnetograph

The magnetograph of the Kitt Peak National Observatory has been described by Livingston et al. (1976). It provides daily full-disk longitudinal magnetic field maps. We use a magnetogram taken on July 11 at 15:55 UT in the 868.8 nm line (Fig. 1b [Pl. 6]). This observation is used for computing the coronal magnetic field lines by extrapolation (see next section). The spatial resolution of the magnetogram is around 1". The saturation level of the instrument is about 9000 G; however, because of scattered light, the response of the system inside sunspot umbras was reduced by about a factor of 1.5 (J. Harvey, private communication). Taking this correction into consideration in the spots does not change significantly the extrapolated field lines related to the X-ray–bright loops.

3. ACTIVE REGION 6718

AR 6718 during its disk passage was followed by Debrecen and Potsdam observatories (Aurass et al. 1993). AR 6718 appeared at the east limb as a fairly regular bipolar group, consisting of a round middle-sized spot on the preceding end, together with an elongated (NW-SE) following part with several umbrae in a common penumbra on the other end, and some pores in the middle of the group. The most stable two umbrae are named P0 and F0, as shown in Figure 1a. On July 7, F0 is separated from the rest of the

chain by a light bridge, while the other umbrae of the following part gradually decrease and disperse.

A development of new activity begins from July 8 to 9. In the middle part of the active region, there are new pores forming continually, mostly of positive polarity, which stream forward systematically and eventually coalesce with P0. On July 10, four small umbrae appear and form P1. The counterpart of P1 may be F1 to the south of F0. South of F0, small satellite sunspots of positive polarity emerge, which will correspond to some bright points seen in X-rays during the rocket flight. To the east of F0 we observe a sunspot, P4, which is also associated with X-ray brightenings. At the center of the active region, the small dipole consisting of the pores P2 and F2 is observable only on July 11.

The axis of the new emerging flux regions P1–F1 and P2–F2 has a significant shear compared with the P0–F0 axis (Fig. 2). Their evolution is responsible for the flare occurring on July 10. The greatest evolution is from July 10 to 11 (Aurass et al. 1993). The two ribbons were over P1 and F1, and the flare is likely due to the interaction of P1–F1 with P0–F0. Microwaves at high frequency were recorded. This active region is not very productive of the high level class of flares. Geophysical Data registered the following:

1. July 9, 15:04 M1.2 and some C flares;
2. July 10, 12:26 UT M3.6 and some C flares;
3. July 11, 13:39 and 14:54 UT Hα subflares;
4. July 12, some C flares.

During the NIXT flight, no flares occurred in this region, but sheared bright loops were observed over the active
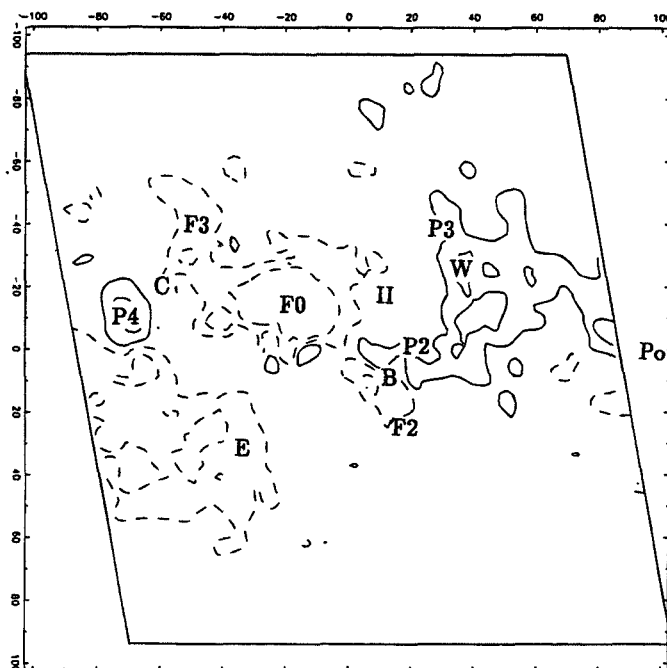

FIG. 2.—Kitt Peak magnetogram of AR 6718 centered on the larger X-ray loops. The labels (P0–P4, F1–F3) designate the sunspots (see Fig. 1) according to their magnetic polarities, "II" locates the Hα filament (from Aurass et al. 1993), while B, C, E, W locate the main X-ray structures (from Golub et al. 1994). Continuous and dashed isoncontours represent the longitudinal photospheric field (100 G, 400 G). The scale length unit is in Megameters. North is to the top. The diamond frame delimits the part of the magnetogram shown in the following figures; its borders are parallel to the local parallel and meridian. The extrapolation computation however, is done for a larger region (400 Mm).
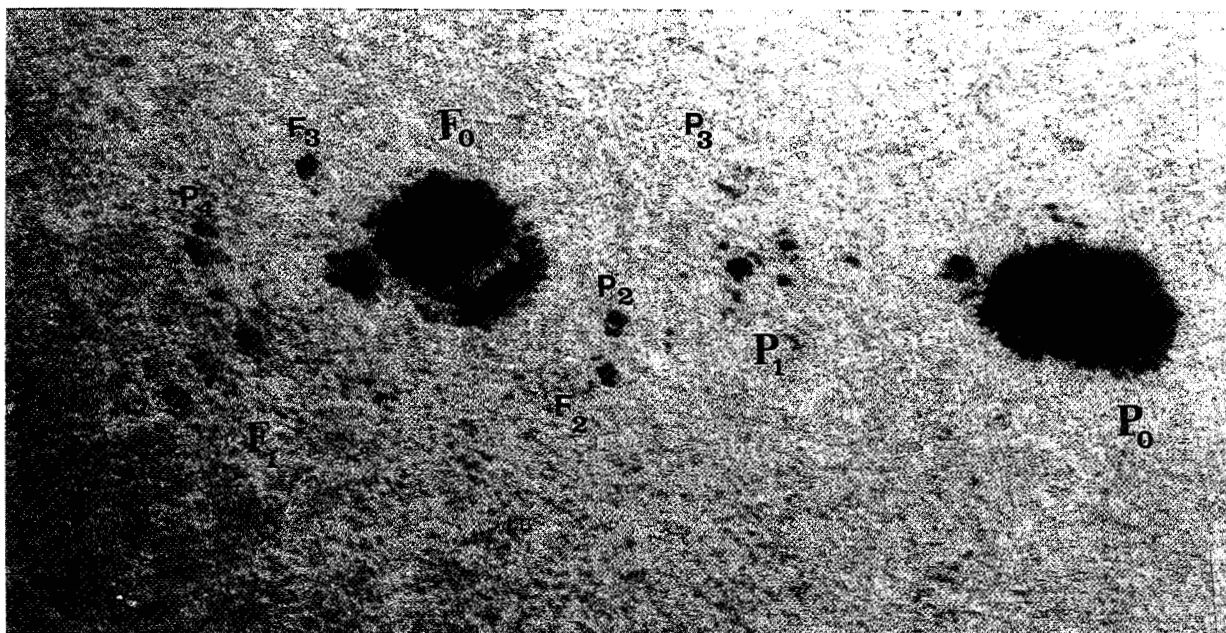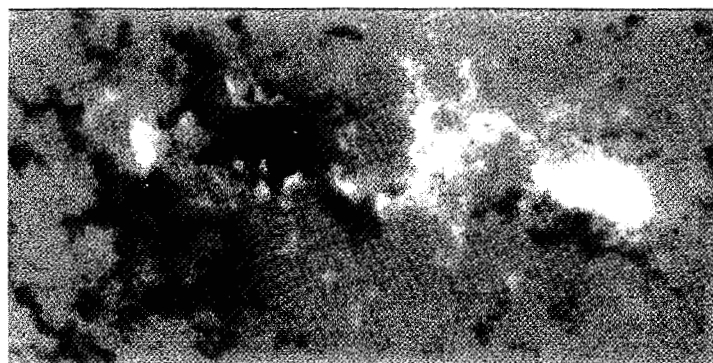
PLATE 6

FIG. 1a

FIG. 1b

FIG. 1.—(a) White-light image of AR 6718 obtained in Débrecen (courtesy of B. Kalman). The letters indicate the sunspots according to their magnetic polarities and relationship. (b) Kitt Peak magnetogram of AR 6718. White/black regions correspond to positive/negative polarities (courtesy of J. Harvey).

SCHMIEDER et al. (see 467, 882)

region. We propose computing the extrapolated magnetic field in the corona from photospheric observations in order to quantify the shear of the coronal loops observed in X-rays.

4. EXTRAPOLATION OF THE MAGNETIC FIELD

The extrapolation code is based on the work of Alissandrakis (1981). The extrapolated fields are calculated under the linear (or constant α) force-free field assumption ($\nabla \times \mathbf{B} = \alpha \mathbf{B}$) using a fast Fourier transform method. (Fig. 3). The required boundary condition is a match to the longitudinal magnetic field values at the photosphere. In order to be able to extrapolate the large-scale structures that are the X-ray–bright loops present in AR 6718, a magnetogram with a large field of view is required. We select a region approximately 400 by 400 Mm in the full-disk Kitt Peak magnetogram. In the figures, we show only a fraction of this field of view, corresponding to the large-scale X-ray loops approximately 100 Mm long, but the magnetic computations are always done using the full selected magnetogram region. This extended region was required to take into account the surrounding field and to decrease the aliasing errors at the borders of the computed region (see Alissandrakis 1981).

The use of magnetograms taken away from the solar disk center requires the elimination of projection effects on the magnetic field and on the spatial coordinates. The full transformation method has been discussed by Gary & Hagyard (1990). On this base, Démoulin et al. (1996) have developed a three-dimensional code for magnetic extrapolation; it has been applied to relate Hα flare brightenings to the magnetic topology of the extrapolated field. A more detail discussion of the extrapolation procedure and tests can be found there.

In the present case, the spiral pattern of Hα fibrils indicates that the fields at the chromospheric level are not potential (see Aurass et al. 1993 or Fig. 4a [Pl. 7]). The presence of magnetic shear at the coronal level is also evident from the X-ray data (Golub et al. 1994 or Fig. 4c). This contrasts with several previous studies, which concluded that quiet coronal structures are well represented by a potential field extrapolation (Poletto et al. 1975; Sams et al. 1992). Therefore, we have investigated the quality of an extrapolation of the magnetogram with increasing values of the shear (Fig. 3). As is evident, the field lines computed from a potential-field approximation cannot represent both the observed Hα and X-ray structures (Figs. 4a and Fig. 4c respectively). As we impose an increasing positive α, the computed field lines become closer to the observed structures. The combination of Hα (showing mainly low-lying loops or the feet of loops), X-rays (showing the coronal part of the loops, but with a varying sensitivity along the loop), and extrapolation (giving the entire field line but with uncertainties in the modeling) permit a clarification of the magnetic configuration of AR 6718.

Connections between the strongest polarities (P0–F0) are found in the extrapolation. But while this is the most important magnetic linkage in AR 6718 (both in magnetic flux and intensity), there is no detectable enhanced heating associated with it, either at the chromospheric or coronal level. Small emerging flux regions, like P2–F2 which emerged from July 9 to 11 (see Fig. 2), produce higher levels of X-ray emission (see Fig. 4c), showing that strong magnetic intensity is not a prime requisite for heating. The magnetic loops connecting P2–F2 were found easily in the

extrapolation but not the ones connecting P3 to F3 (suggested by Aurass et al. 1993): field lines starting from P3 always end to the north of F0.

In the east part of the region, both the X-ray (called C in Golub et al. 1994) and Hα brightenings located to the southeast of F3 are related to magnetic field lines linking F3 to the southeast negative polarity (called P4 in Fig. 2). It is probably the emergence of this bipole P3–F3, like in the above case P2–F2, that leads to forced reconnection with the overlying magnetic field. Other smaller examples of this phenomenon, at lower spatial scale length, are present to the south of F0 (see the small positive polarities in Fig. 2, which are located in close proximity to the small X-ray brightenings).

AR 6718 is thus formed by a great number of dipoles of different scales which reconnect and brighten when they find their way into the corona. This explanation can hardly be generalized to the spectacular X-ray loops extending from east to west because the polarities look well formed and the X-ray loops seem to fill a large coronal volume. Hereafter we focus on that large feature, keeping in mind that the intense X-ray feature called B (Fig. 2) is linked to the emergence of polarities P2–F2 and only seems to be cospatial with the loops extending from west to east because of projection effects.

The hot loops extending from west to east can be found in the field line extrapolation when a positive α is introduced (Fig. 3). However, a unique value of α will not fit all the observed structures. Larger and higher structures are found to be less sheared than the lower ones, and even the very low highly sheared structures seen in Hα in the vicinity and in the Hα filament (indicated by II in Fig. 2 and visible in Fig. 4a) cannot be reproduced by the extrapolation. Here we see a paradox between the observations and the linear force-free field model. An intrinsic property of the linear force-free field is that large structures are more sheared than smaller ones, implying that long field lines become unrealistically distorted as α is increased (Fig. 3), while short low-lying loops cannot be made as sheared as they are observed to be. The comparison of observations to the extrapolation shows that the coronal magnetic field is not in a state of minimum energy (which is a linear force-free field keeping the total magnetic helicity preserved).

Within the limits of the constant α hypothesis, we can nevertheless reproduce the observed shape of the X-ray loops. The lower loops, corresponding to the dash-dotted curves in Figure 4b, are reproduced in the extrapolation by using $\alpha = 0.019$ Mm^{-1}. The larger loops, corresponding to the continuous curves in Figure 4b, are approximately reproduced in the extrapolation with $\alpha = 0.013$ Mm^{-1} ($\approx 30\%$ less than the value requires for the lower X-ray loops). These loops are still highly sheared, and they extend to a large altitude (between 60 and 100 Mm). One can imagine that there are magnetic loops which extend even higher, becoming progressively closer to the potential case, but that such loops are not bright enough to be seen in X-rays. A simplified model of this region is a system of magnetic arcades, highly sheared in the center and becoming progressively less sheared outward (Fig. 5). This is in agreement with the schematic view of the magnetic configuration that Martin (1990) proposed for magnetic configurations supporting filaments.

But why are the loops that extend from west to east bright in X-rays? The brightness of the footpoints both in
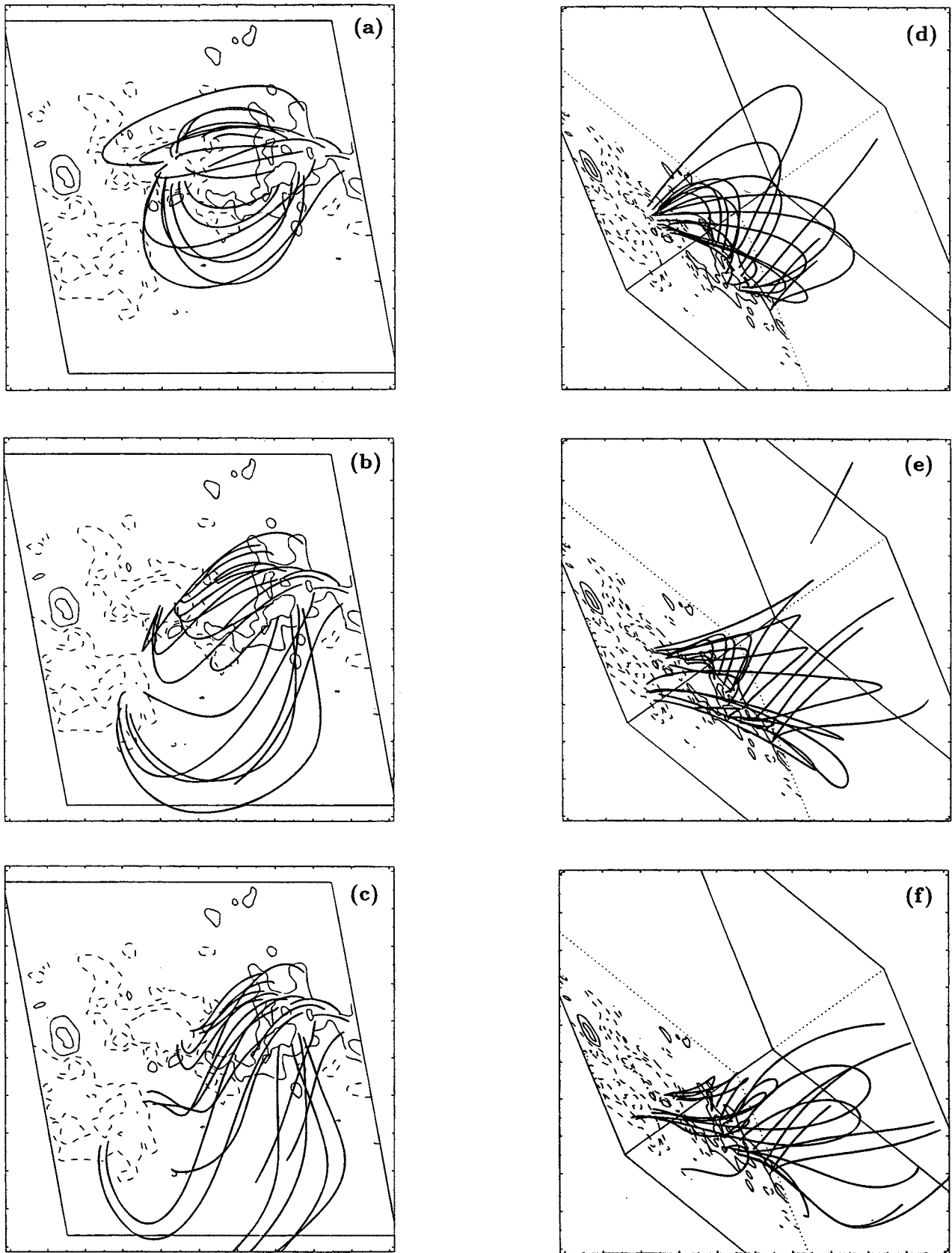
FIG. 3.—Extrapolation of a Kitt Peak magnetogram of the AR 6718 with (*a, d*) a potential field and a linear force-free field with (*b, e*) $\alpha = 0.013$ Mm^{-1} and (*c, f*) $\alpha = 0.019$ Mm^{-1}. Field lines have the same starting footpoint in the positive polarity. In (*a–c*), the point of view of the observer is used (north is to the top), while in (*d–f*) a side view is shown with the same field lines. The drawing convention for the longitudinal field is the same as in Fig. 2. Only a local view of the region is shown, but the extrapolation is made on a region 4 times larger.

PLATE 7
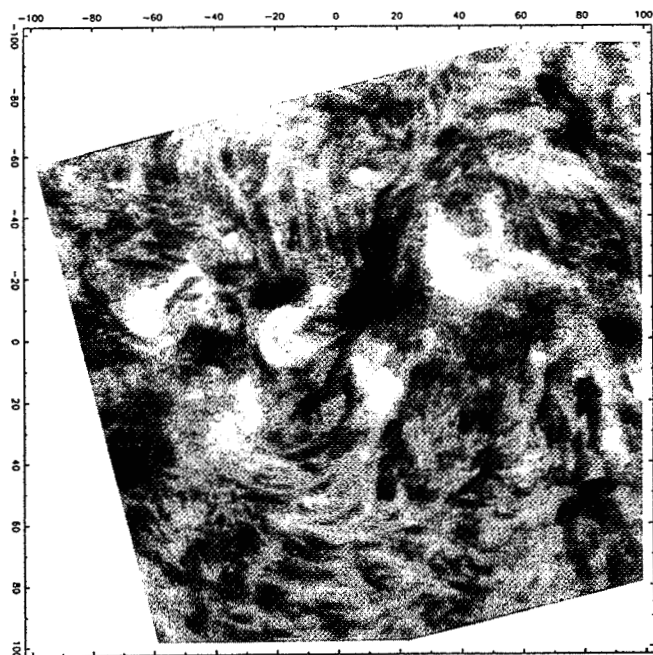
FIG. 4a
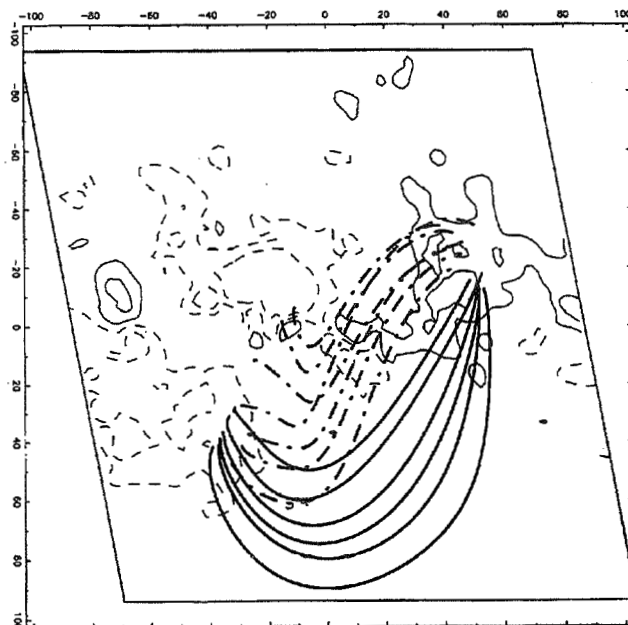
FIG. 4b
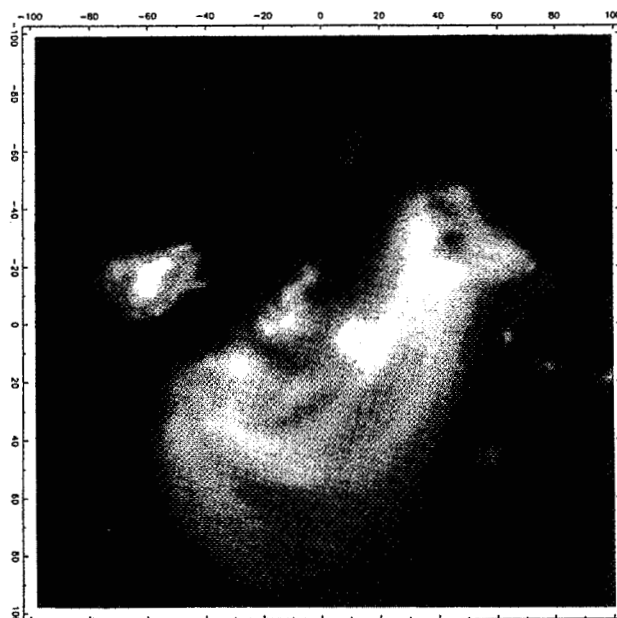
FIG. 4c

FIG. 4.—Comparison of (a) the MDSP and (c) the NIXT observations of AR 6718 to (b) the field line computation. The computed field lines (drawn in continuous style) have a shape compatible with the largest X-ray–bright loops only when a sheared field is used ($\alpha = 0.013$ Mm^{-1}). The interpretation of the shape of the lower X-ray loops by field lines (drawn in dash-dotted style) requires a slightly more sheared field ($\alpha = 0.019$ Mm^{-1}). The degree of magnetic shear decreases with height from the lower highly sheared Hα loops (a) to the higher coronal loops (c).
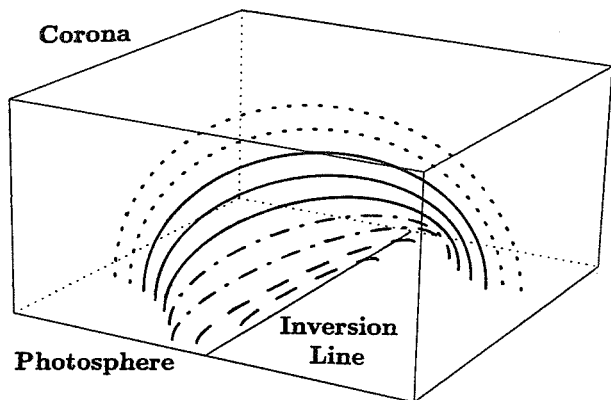
SCHMIEDER et al. (see 467, 883)

FIG. 5.—Schematic view of the magnetic configuration of AR 6718. The prominence is present in low-lying highly sheared loops (*dashed lines*), surrounded by arcade loops with magnetic shear decreasing with height (field lines corresponding to the observed X-ray coronal loops are drawn with dash-dotted and continuous lines, while the supposed overlying more potential field lines are drawn with dotted lines).

Hα and X-rays delineates approximately the magnetic field map, in particular for the characteristic shape of P3 (Fig. 4). But we have seen above (for loops connecting P0 to F0) that the magnetic field strength is not sufficient to determine the X-ray brightness. The shape of the loop footpoints tells us only that the energy is of magnetic origin and that some other physical parameters should play a key role. It could be the topology of the magnetic field: it is well known that magnetic reconnection occurs on separatrices (see, e.g., Van den Oord 1993; Démoulin 1994). Therefore, we have tried an analysis similar to the one carried out for flares (Démoulin et al. 1996), but without success. This may indicate that the magnetic topology is not well represented by our computation in this highly sheared region (in particular because magnetic shear decreases with height, while the opposite occurs in the linear force-free field extrapolation). But, rather than a localized emission on some loops (or flat volume), the observed X-ray loops on July 11 are seen in a large volume. Another possibility, as suggested in a recent study by Moore et al. (1994), is that X-ray loops are heated at the places at which high shear is present and where underlying flux cancellation occurs. In the present event, flux cancellation may happen in the small bipole (P2–F2) under the large-scale X-ray loops, but it is difficult to believe that such localized and low-lying phenomena can trigger magnetic energy release in the whole large-scale set of X-ray loops.

Rather, we propose that the origin of the observed brightenings of the strongly sheared region are due to the relaxation of the magnetic field as modeled by Heyvaerts & Priest (1984). They described how a magnetic field can lose its excess energy via an MHD turbulent process. In a highly conducting plasma, small-scale processes dissipate magnetic energy much more rapidly than the total magnetic helicity ($H = \int AB \, dV$ with $B = \nabla \times A$; Taylor 1974) or more precisely in the solar context, the total relative helicity (Berger 1985, and references therein). With this constraint, the magnetic field does not relax to a potential state but to a linear force-free state (as was observed in laboratory experiments in spheromacs (Rosenbluth & Bussac 1979). The theoretical final state of the process is a magnetic field with constant α. The gradient of α found in this region (scale

length of 100 Mm) shows that the process of relaxation was not complete at the time of the observations.

5. DISCUSSION AND CONCLUSION

We have used a linear-force-free field extrapolation of the longitudinal field to understand the three-dimensional shape of the observed X-ray and Hα structures. The X-ray loops in AR 6718 can be separated in two sets: compact and small loops (with an extension lower than 30 Mm) and large loops (extending to greater than 100 Mm). The emergence of small parasitic polarities and the reconnection of this new magnetic flux with the preexisting coronal magnetic field is the most plausible interpretation for the small-scale X-rays and Hα brightenings. The large-scale X-ray loops are anchored in the bipolar field (P1–F1) located in the middle of a stronger bipolar field (P0–F0). Only a set of loops joining P1 to F1 is observed to be bright in X-rays. These loops cannot be related to field lines in the potential approximation, but we show, in a first approximation, that a constant α force-free field extrapolation permits their shape to be recovered, and it shows that the large-scale X-ray loops are highly sheared. However, a second approximation step shows that a different α value is required to fit the field lines both to the lower and upper parts of the X-ray loops. The upper ones are less sheared; they require an α value approximately 30% smaller than for the lower loops. Moreover, an Hα filament is present below and the Hα fibrils are nearly aligned along the photospheric inversion line, showing that the central part is strongly sheared. Then X-ray and Hα observations combined with the magnetic extrapolation show that the central part of AR 6718 is formed by a highly sheared magnetic field, with a magnetic shear decreasing progressively with height (on a scale height of the order of 100 Mm). Therefore, we propose a differential shear configuration for the magnetic field, with a strongly sheared core (Fig. 5), in agreement with the views of Martin (1990) and Antiochos, Dahlburg, & Klimchuk (1994).

The small-scale X-ray loops can find their origin in the reconnection of parasitic flux with the preexisting magnetic flux, while the brightness of the large-scale X-ray loops is puzzling. In the large-scale magnetic configuration, why are only some loops bright? The magnitude of the magnetic field is not the only important parameter of the heating mechanism, since some parts of the corona have much higher fields while they do not emit in X-rays, and the X-ray–bright loops do not have footpoints in the main sunspots (see also Sams et al. 1992). However, we can surmise that the mechanism is of magnetic origin, since the brighter loops are associated with the photospheric magnetic polarities. Are the observed loops bright due to reconnection between the main bipoles (P0–F0) and (P1–F1)? Within the limits of the magnetogram calibration and the linear force-free field assumption, the topological computations have failed to explain the position of the large X-ray loops. Moreover, the observed spatial extension of the bright loops rules out a mechanism localized on a very flat volume, like reconnection on two intersecting separatrices. The mechanism for heating these quiet X-ray loops seems to be different from that found for flares (Démoulin et al. 1996).

We find that the brightest soft X-ray emission corresponds to a nonpotential state of the magnetic field, in which the strongest X-ray emission is associated with the largest shear (this, however, does not hold for the highly

sheared field lines containing the filament). This agrees with Moore et al. (1994), who report that the coronal heating is enhanced at the sites of strong shear. This argument receives additional indirect support from the measurement of the cross-sectional variation of the loops observed by NIXT (Golub 1991) and by the *Yohkoh* SXT: the thickness variation along the loop was found to be only 10%–20% at most. McClymont & Mikic (1994) demonstrate that this observation is consistent with the characteristics of current carrying field lines in a highly sheared active region (using an MHD code for the extrapolation). The relationship between electric currents and X-ray brightness (and therefore heating) is, however, still debatable. Metcalf et al. (1994) find no correlation between the locations of bright X-ray structures and the sites of sustained strong photospheric currents; the field lines connecting the upward/downward current densities are found to be unassociated with the brightest SXR emission over a 7 day period of observation. For AR 6718, present vector magnetographs like the one in Potsdam are not sensitive enough in the linear polarization to derive electric currents at the feet of the large X-ray loops at which the strength of longitudinal magnetic field is low (≤ 400 G at the magnetograph resolution).

The central part of AR 6718 is formed by a highly sheared magnetic field, with a magnetic shear decreasing progressively with height. This differential shear may be at the origin of the observed loop brightening, triggering a relaxation process as proposed by Heyvaerts & Priest (1984).

With the high magnetic Reynolds number of the solar corona, the total magnetic helicity of the magnetic field is preserved. With this constraint, a stressed magnetic field relaxes, via MHD turbulence, to the linear force-free field compatible with the boundary conditions (mainly the photospheric vertical flux distribution). Following Moore et al. (1994), the magnetic shear could be a necessary condition, but not a sufficient one for heating. A differential magnetic shear is likely to be another condition. Finally, a multitude of reconnecting current sheets, the dissipation of a large number of small-scale currents, or a wave heating mechanism are possible alternatives, but the present data cannot permit a definitive selection of all the possible candidates for coronal heating mechanisms.

REFERENCES

Alissandrakis, C. E. 1981, A&A, 100, 197
Antiochos, S. K., Dahlburg, R. B., & Klimchuk, J. A. 1994, ApJ, 420, L41
Aurass, H., Hofmann, A., Magun, A., Soru-Escaut, I., & Zlobec, P. 1993, Sol. Phys., 145, 151
Berger, M. A. 1985, ApJS, 59, 433
Démoulin, P. 1994, in Advances in Solar Physics, ed. G. Belvedere, M. Rodono, & G. M. Simnett (Berlin: Springer), 121
Démoulin, P., Bagalá, L. G., Mandrini, C. H., Hénoux, J. C., & Rovira, M. G. 1996, A&A, submitted
Gary, G. A., & Hagyard, M. J. 1990, Sol. Phys., 126, 21
Gary, G. A., Moore, R. L., Hagyard, M. J., & Haisch, B. M. 1987, ApJ, 314, 782
Golub, L. 1991, in Mechanisms of Chromospheric and Coronal Heating, ed. P. Ulmschneider, E. R. Priest, & R. Rosner (Berlin: Springer), 115
Golub, L., Zirin, H., & Wang, H. 1994, Sol. Phys., 153, 179
Hannakam, L., Gary, G. A., & Teuber, D. L. 1984, Sol. Phys., 94, 219
Heyvaerts, J., & Priest, E. R. 1984, A&A, 137, 63
Livingston, W. C., Harvey, J., Slaughter, C., & Trumbo, D. 1976, Appl. Opt., 15, 40
Martin, S. 1990, in IAU Colloq. 117, Dynamics of Quiescent Prominences, ed. V. Ruzdjak & E. Tandberg-Hanssen (Lecture Notes in Physics, Vol. 363), 1

McClymont, A. N., & Mikic, Z. 1994, ApJ, 422, 899
Mein, P. 1977, Sol. Phys., 54, 44
Metcalf, T. R., Canfield, R. C., Hudson, H. S., Mickey, D. L., Wülser, J. P., Martens, P. C. H., & Tsuneta, S. 1994, ApJ, 428, 860
Metcalf, T. R., Jiao, L., McClymont, A. N., Canfield, R. C., & Uitenbroek, H. 1995, ApJ, 439, 474
Moore, R. T., Porter, J., Roumeliotis, G., Tsuneta, S., Shimizu, T., Sturrock, P. A., & Acton, L. W. 1994, Proc. Kofu Meeting (NRO Rep. No. 360), 89
Peres, G., Reale, F., & Golub, L. 1994, ApJ, 422, 412
Poletto, G., Vaiana, G. S., Zombeck, M. V., Kriefer, A. S., & Timothy, A. F. 1975, Sol. Phys., 44, 83
Rosenbluth, M. N., & Bussac, M. N. 1979, Nucl. Fusion, 19(4), 489
Sakurai, T. 1982, Sol. Phys., 76, 301
Sakurai, T., & Uchida, Y. 1977, Sol. Phys., 52, 397
Sams, B. J. III, Golub, L., & Weiss, N. O. 1992, ApJ, 399, 313
Schmieder, B., Dere, K. P., Raadu, M. A., Démoulin, P., & Alissandrakis, C. E. 1990, Adv. Space Res., 10(9), 195
Schmieder, B., Golub, L., & Antiochos, S. K. 1994, ApJ, 425, 326
Spiller, E., McCorkle, R. A., Wilczynski, J. S., Golub, L., Nystrom, G., Takacs, P. Z., & Welch, C. 1991, Opt. Eng., 30, 1109
Taylor, J. B. 1974, Phys. Rev. Lett., 33, 1139
Van den Oord, G. H. J. 1993, Adv. Space Res., 13(9), 143

DIFFICULTIES IN OBSERVING CORONAL STRUCTURE

L. GOLUB

Smithsonian Astrophysical Observatory, Cambridge, MA 02128, U.S.A.

Abstract. There has developed in recent years a substantial body of evidence to indicate that the temperature and density structure of the corona are far more complicated than had previously been thought. We review some of the evidence and discuss some specific examples: observations of a limb flare, showing that the cool Hα material is *cospatial* with the hot X-ray emitting material; simultaneous NIXT and *Yohkoh* SXT observations of an active region, showing that loops seen in one instrument are not seen in the other, and that the effect works in *both* directions; comparisons of extrapolated magnetic field measurements to the observed coronal structure, indicating that neither potential nor constant-α force-free fits are adequate. We conclude with a description of two new instruments, the TRACE and the TXI, which will help to resolve some of these difficulties.

1. Overview

The importance of magnetic fields in determining the structure of the solar outer atmosphere has long been recognized. Billings (1966) notes that magnetic fields 'are employed, as a matter of fact, to explain all departures from a nonspherical [sic] distribution of matter in the corona, including the loop structure of the corona over active regions...' Observations from sounding rockets in the late 1960s and early 1970s provided convincing evidence that loops structures, apparently outlining the magnetic field direction, are fundamental (Vaiana, Krieger, and Timothy, 1973) and the *Skylab* observations in 1973-1974 provided the impetus for constructing atmosphere models in which loop 'mini-atmospheres' are the fundamental constituent of the inner corona (Rosner, Tucker, and Vaiana, 1978; Craig, McClymont, and Underwood, 1978).

This atmosphere is dynamic and constantly varying. Low (1990) notes that the solar atmosphere is never truly quiescent or static, but adds that for the purpose of building models idealized static states may be used as an approximation to the physics underlying the apparent stability of long-lived structures. The extremely dynamic nature of the corona has been shown most effectively by the Soft X-ray Telescope (SXT) aboard the *Yohkoh* satellite: repeated transient loop brightenings in active regions (Shimizu *et al.* 1992), continual rapid expansion outward of structures at the tops of active regions (Uchida *et al.*, 1992), jets of X-ray emission, apparently associated with reconnection events (Shibata *et al.*, 1992), among others.

Thus, it is already clear that the simplest models of the corona – spherical or plane-parallel – are of limited applicability for interpreting the actual observations, and that the simplest loop atmosphere models – static loops – are also of limited usefulness. To these complications, we will add an additional set of worries, by

CORONAL STRUCTURES OBSERVED IN X-RAYS (NIXT) AND Hα SURGES

B. Schmieder [1], Z. Mouradian [1], L. Golub [2], S. Antiochos [3]

[1] *Observatoire de Paris, Section Meudon, 92195 Meudon, France*
[2] *Harvard-Smithsonian Center, 60 Garden Street, Cambridge, MA 02138, U.S.A.*
[3] *Naval Research Laboratory, Washington, DC 20375, U.S.A.*

Abstract

Ground-based coordinated observations with the Multichannel subtractive double pass spectrograph (MSDP) and the heliograph in Meudon allowed us to portray the chromospheric intensity and velocity fields below coronal structures observed with the Normal Incidence X-ray Telescope (NIXT). On July 11, 1991 (eclipse day) we have identified in AR 6713 (N38 W 42) the X-ray signatures of the network, subflares, filaments and surges. The largest Hα surge has only weak emission in X-ray, while a weak Hα feature corresponds to a very bright x-ray subflare. We calculate the emission measures of these events and give some constraints on the triggering mechanisms of surges.

1. Introduction and Observations

The observations have been described in details by Schmieder *et al.* (1993, 1994a,b). We shall report them briefly. A recurrent surge (S) has been observed with the Meudon heliograph (Fig. 1). The figure 2 displays the X-ray image observed by NIXT at 63.5 Å, sensitive at $T = 1$ and 3×10^6 K in the top pannel and in the bottom pannel the Hα image (composite of intensity and velocity) obtained with the MSDP operating at Meudon. The letter S indicates the large Hα surge and the X-ray weak signature, the letter G the X-ray microflare and the Hα weak intensity signature. Along the surge S and in G large Hα flows are detected. The microflare G is directly related to a chromospheric dynamical event. This may be an exemple of dynamism without evident energy transport.

2. Model

The data set described above provides a unique opportunity to test models of surges and, in particular, models in which the motions are driven by gas pressure gradients. The

PROCEEDINGS

OF

KOFU SYMPOSIUM

Edited by
S. Enome
T. Hirayama

*New Look at the Sun
with Emphasis on Advanced Observations
of Coronal Dynamics and Flares*

Kofu, September 6 –10, 1993

B. Schmieder et al.
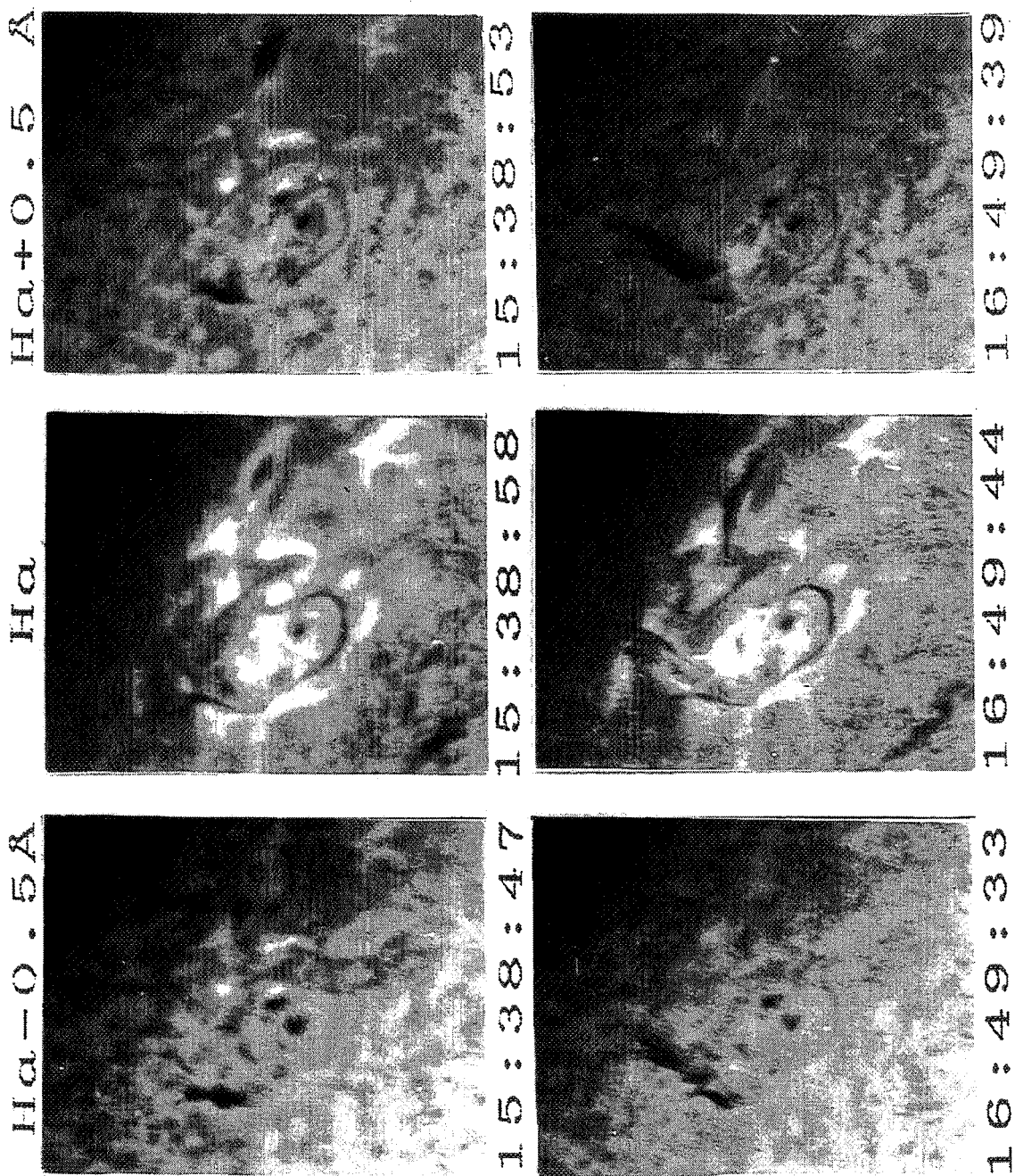
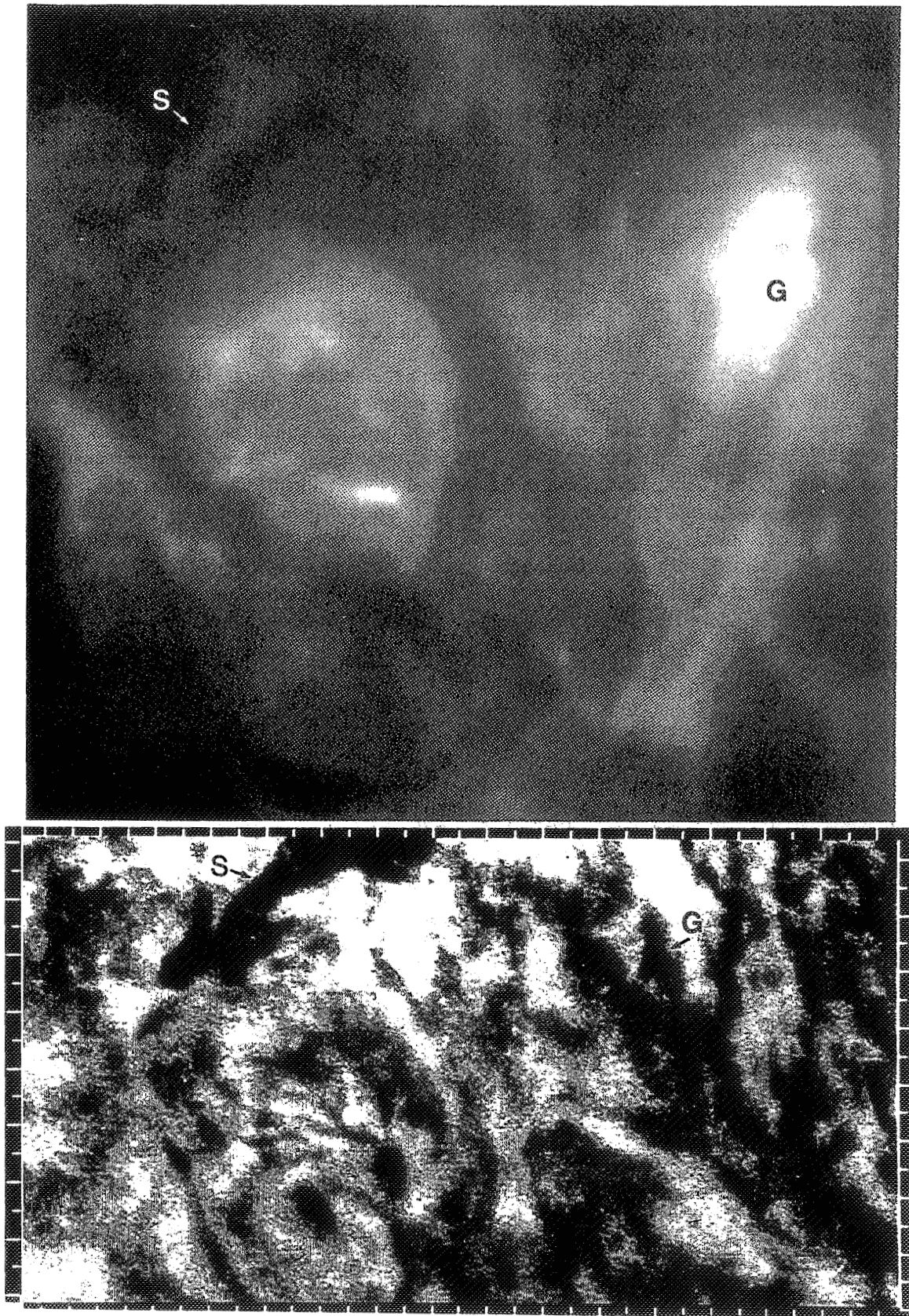Fig. 1. Meudon 3-λ heliograms of AR 6713 on July 11, 1991

Fig. 2. Active region AR 6713 observed in X-ray with the NIXT and in Hα with the MSDP (blue/red corresponds to blue/redshifts)

Table I

Observational questions about the solar corona

Q1.	Is the corona hot or cold at a given point in space?	A1.	Depends on the viewing method.
Q2.	Where is the 'base' of the corona?	A2.	Meaningful only for individual loops and probably unanswerable.
Q3.	What is the transverse scale size of coronal structures?	A3.	Our knowledge is limited by present instrumental resolutions.
Q4.	What is the relation between the coronal B and X-ray emission?	A4.	Data do not provide sufficient constraints.
Q5.	What does the hot corona look like?	A5.	Depends on the viewing method.

showing that it is not at all clear that we are even now in a position to say that we know what coronal loops look like, or to know how the real corona is constructed of such loops.

2. Case Studies

In order to illustrate the difficulties alluded to in the Overview, we will examine five specific 'case studies', each involving a seemingly reasonable question about the corona. The questions addressed by these studies are listed in Table I, along with the answer to each question. The latter will be explained in the course of discussing each case. These examples are all taken from work related to flights of the Normal Incidence X-ray Telescope (NIXT) sounding rocket payload (Golub *et al.*, 1990) during the years 1989–1993.

2.1. A LIMB FLARE

On 11 Sept. 1989, the NIXT rocket was launched at the start of a small flare (GOES classification C5). However, during the five-minute flight, a second flare began in an active region at the limb (Herant *et al.*, 1991). Examination of the GOES X-ray light curves (Figure 1) indicates that the limb flare began at about 16:36 UT during the decay phase of the larger on-disk flare. The NIXT observations also began at 16:36 UT, with the last image taken at 16:41:35 UT; the peak of the limb flare in X-rays is at ∼16:42 UT. Thus, the NIXT coverage could not have been better-timed.

Figure 2 shows simultaneous Hα and X-ray images of the flare at the time of the peak. The most striking aspect of this event seems to be the nearly identical size, shape and location of flare in the two wavelength regimes. This similarity is confirmed by a cross-correlation between the two datasets, shown in Figure 3. The contour lines show the X-ray brightness and the shaded region shows the He brightness: the two overlap to within the accuracy of alignment. Thus it would
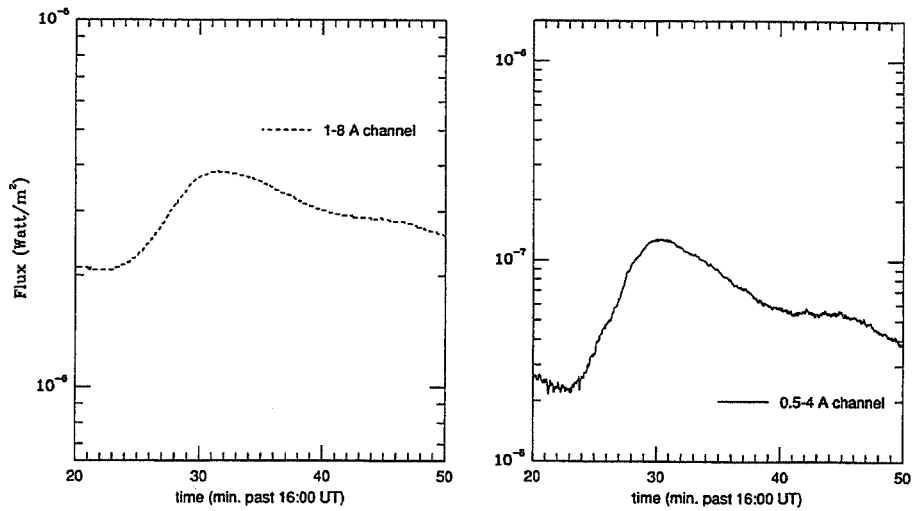
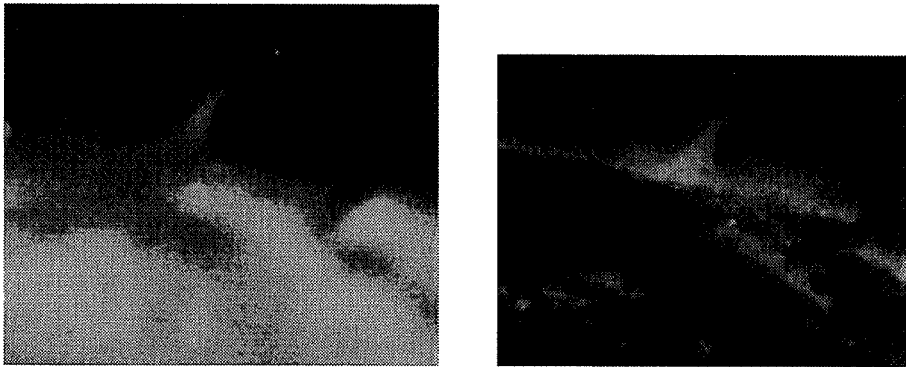*Figure 1.* GOES 1-8 Å and 0.5–4 Å X-ray plots for 9 November, 1989.

Figure 2. Simultaneous Hα and NIXT X-ray images of a limb flare.

appear that the corona is both hot (X-ray) and cool (Hα) at the same place at the same time.

Possible explanations exist, of course, for this apparent contradiciton. It is possible that the X-ray emission originates from a thin shell ahead of the advancing Hα region. Alternatively, hot and cool material may be intermingled on small spatial scales within the observed regions. The problem is not to come up with an answer, it is to come up with a correct answer.
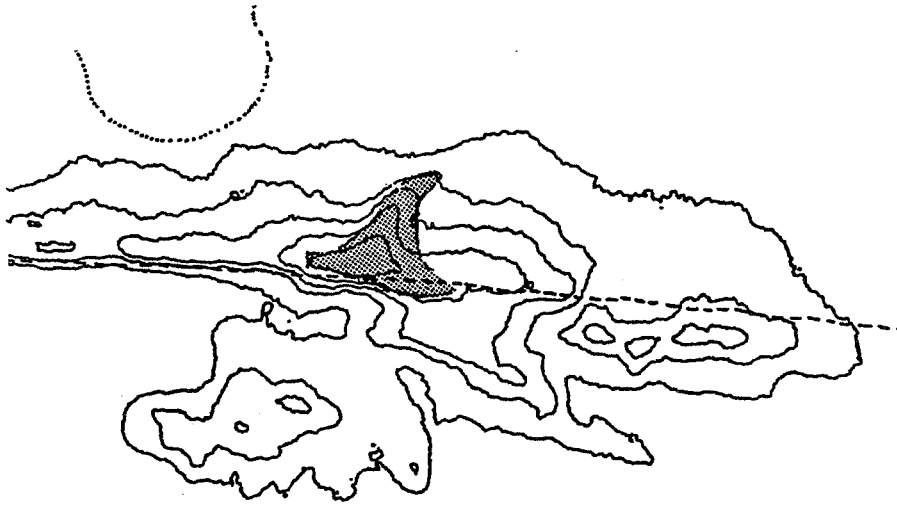
Figure 3. Relative positions of X-ray event and Hα material.

2.2. SIMULTANEOUS WHITE-LIGHT AND X-RAY IMAGING

Plane-parallel, or spherically symmetric models of the outer solar atmosphere treat the relation between temperature and height as one-dimensional, although not monotonic since the temperature at first increases with height but then decreases again. With the advent of loop model atmospheres, as described above, this fundamental view did not change in essence, but the temperature vs height relation is transplanted into each loop instead of into the atmosphere as a whole. However, a flight of the NIXT payload on 22 February 1991 provided a unique dataset which shows that a more complicated geometry is required in order to explain the observations.

The multilayer mirrors used in the NIXT to provide X-ray imaging also reflect visible light with $\approx$ 50% reflectivity. In order to record only the (much fainter) X-ray image, two stages of visible-light rejection are employed: an entrance aperture filter, which cuts the visible to $\approx$ 1% and a focal plane filter, which provides 10^9 reduction in the visible. During the launch phase of the February 1991 flight, a portion of the entrance aperture filter broke. The instrument, however, was designed so that the focal plane filter acts as back-up in the event of just such a failure. Thus, because the X-rays and the visible are reflected in the same way from the same mirror at the same time, we obtained simultaneous images of the visible disk and the corona. These are automatically coaligned and have the same plate scale, so that high precision (<1 arc sec) comparison between the two can be made.

Figure 4 shows a portion of the east limb from one of the exposures obtained on that flight. Note that there is a dark band at the limb, between the white-light solar limb and the bright coronal X-ray emission. We note several features of this
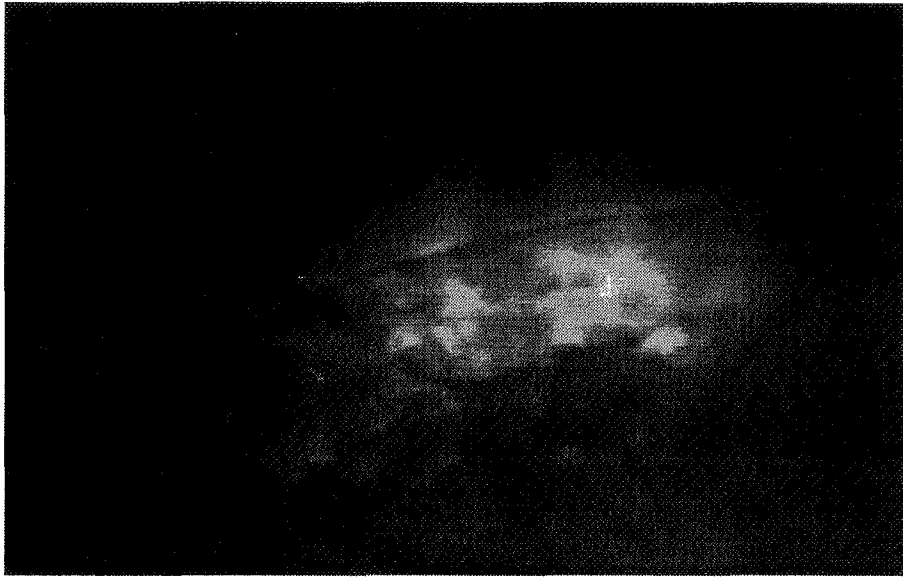
Figure 4. Portion of a combined NIXT/white-light image, showing a gap between the visible limb and the 'base' of the corona, 22 February, 1991.

gap: (1) it is most clearly evident when there is an X-ray emitting region behind the limb and no emitting region in front of the limb; (2) the thickness of the gap varies between equator and poles, or between active regions and large scale 'quiet' regions; (3) at both the inner (white light) and outer (X-ray) heights, the gap is quite sharp. The question we will address is, how is this gap to be interpreted?

The data from this flight have been analyzed by Daw, DeLuca, and Golub (1995), who find that a model in which the corona is viewed as consisting of a homogeneous set of loops, with temperature varying as a function of height in a uniform manner (Figure 5(a)) is not consistent with the data. In order to explain what is seen, it is necessary to use a model in which hot loops penetrate downward into an atmosphere having cool spicular material penetrating upward (Figure 5(b)). The two types of loops do not connect physically, but are interspersed along the line of sight. Thus, the gap is interpreted as the upward extent of spicular material, viewed along the line of sight at the limb and absorbing the X-rays emanating from loops behind the spicules.

We note that the soft X-rays in the NIXT data are strongly absorbed in spicular material, with about 10 arc sec path length required for e^{-1} absorption. The variation in thickness of the band indicates that spicules may extend farther in open field (e.g., coronal hole) regions than in higher temperature closed-loop regions, as reported by Huber *et al.* (1974). This interpretation of the NIXT data suggests that the footpoints of coronal loops cannot, in principle, be seen. When viewed at the limb,
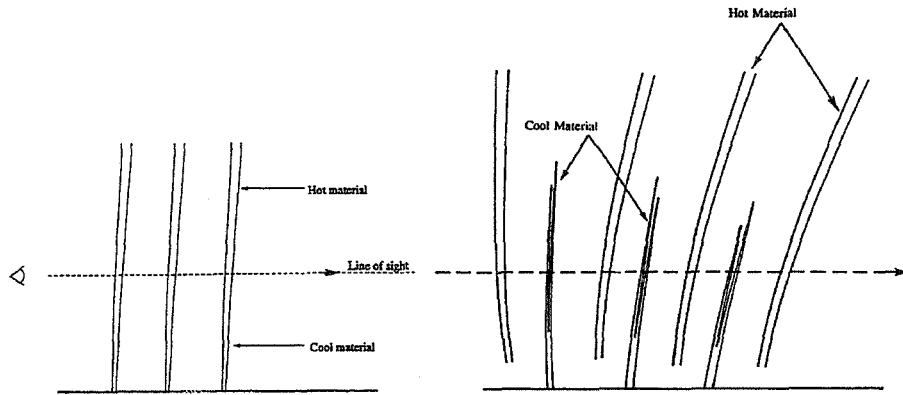
Figure 5. Two loop model atmospheres offering alternative explanations of the gap seen in Figure 4. Modified plane-parallel model on left does not fit the data.

they are obscured by the intervening spicule material; when viewed from above, the projection angle is such that the height of the coronal 'base' is very poorly determined. Depending upon the relative spatial density of hot vs cool structures, there may be a small range of locations near the center of the disk which allow for both viewing the loops at an angle and for viewing them unobstructed. However, this is not yet known.

2.3. ACTIVE REGION FINE STRUCTURE

The progress in X-ray optics, when applied to solar coronal imaging, has consistently revealed coronal fine structure down to the resolution limit of the observing instruments (see, e.g., articles by Giacconi, Golub, and Walker *et al.* in Linsky and Serio, 1993). An example is shown in Figure 6, a coronal X-ray image from the NIXT instrument, obtained on 11 July, 1991. There is clearly fine structure prevalent everywhere in the image and photographic analysis indicates that it reaches the combined limit set by the film and by the pointing stability of the rocket.

A quantitative analysis of the fine structure of several active regions observed by the NIXT was carried out by Gómez *et al.* (1993). By Fourier analyzing the images, they find a broad, isotropic power-law spectrum for the spatial distribution of soft X-ray intensities. The spectrum has a slope of $\alpha \approx -3$, which extends down to the resolution limit of the instrument at ≈ 0.75 arc sec.

A similar result has been obtained by Martens and Gómez (1992) from analysis of *Yohkoh* SXT data: the Fourier transform distribution is a power law (with somewhat smaller slope of ≈ -2.4) which extends down to the Nyquist frequency. Thus, for both cases in which the procedure has been carried out, the spatial structuring of the corona is seen to be limited by the resolution of the imaging instrument. The implication, since the sun does not know what instrument we are
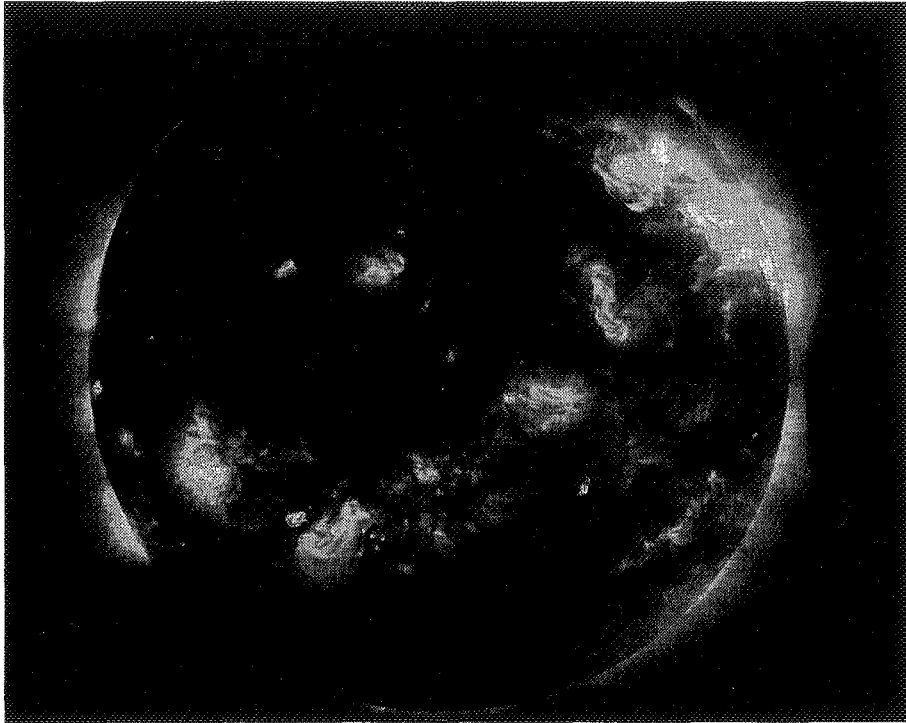
Figure 6. 11 July, 1991 NIXT image.

using to observe it, is that we have not yet fully resolved the coronal fine structure. Thus, the answer to Question 3, 'What is the transverse scale size of coronal structures?', is that we do not yet know.

2.4. Magnetic Field Extrapolation vs Observed Structure

There have been only a limited number of attempts in recent years to carry out direct comparisons between high resolution coronal observations and magnetic field extrapolations, if we exclude attempts to explain the onset of flares by testing the non-potentiality of fields. For non-flaring regions, i.e., normal coronal structure, Poletto *et al.* (1975) and Sakurai and Uchida (1977) had reasonable success at the level of late 1960s and early 1970s resolution. More recently Sams *et al.* (1992) found a general agreement between extrapolations and the structures seen in the NIXT, although close examination shows that the agreement is quite poor in detail. Metcalf *et al.* (1994) conclude, from comparison of vector magnetograph data (giving the locations of vertical currents) with *Yohkoh* SXT coronal data, that there is a very por spatial and temporal correlation between the locations of the currents and the locations of bright coronal structures.
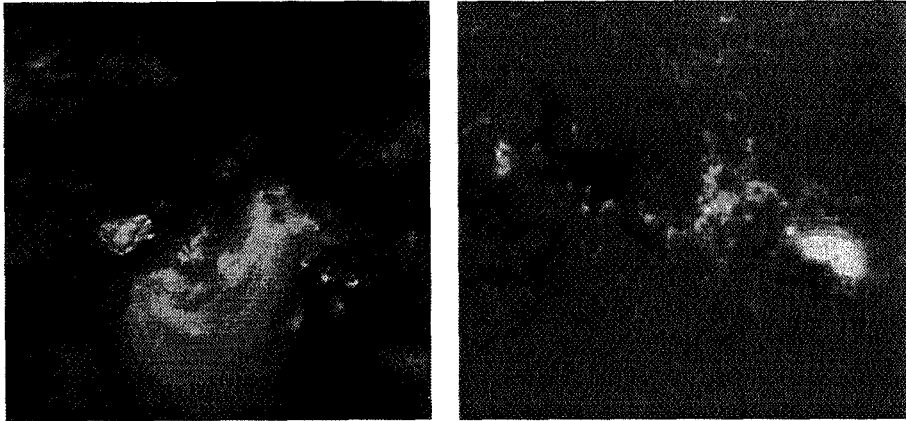
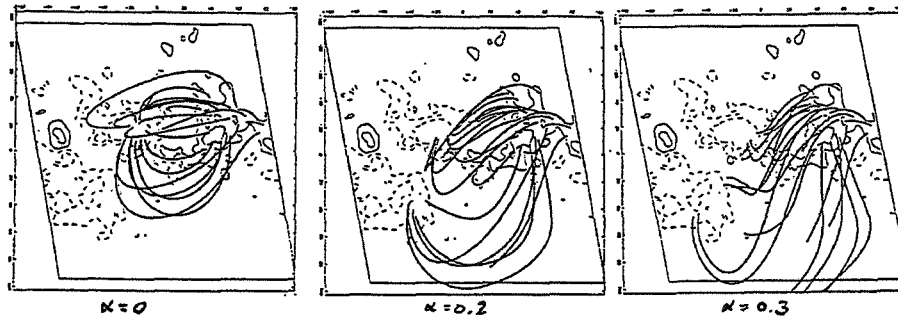*Figure 7.* NIXT X-ray image of AR 6718 and KPNO magnetogram of the region.

Figure 8. Magnetic field extrapolations of AR 6718, with three values of α.

In a recent study, Schmieder *et al.* (1996) have used high resolution NIXT data combined with Kitt Peak magnetogram and Multi-channel Double Pass (MSDP) spectrograph data, to study in more detail the relationship between the observed structure and the type of magnetic field extrapolation employed. The extrapolation code is based on the work of Alissandrakis (1981) as modified by Démoulin *et al.* (1996). A single active region, AR 6718 on 11 July, 1991, was chosen for study; an X-ray image of the reigon and the corresponding portion of the magnetogram are shown in Figure 7.

The first result is that a potential-field extrapolation does not represent the observed coronal structure at all, and that even a constant-α force-free field extrapolation is not adequate. Figure 8 shows extrapolations using three values of α. The left-most panel shows $\alpha = 0$, i.e., a potential field. Note that the connectivity of the field lines is entirely different from that of the observed structures. The two force-free fits in the middle and right-hand panels match portion of the region, but neither one in itself is a good fit. What we find is that the inner portion of the

active region is well matched by the larger value of oe while the outer portion of the region is matched by a lower α.

A possible interpretation of this result is that there is, with time, a relaxation of the magnetic field, as proposed by Heyvaerts and Priest (1984). In a highly-conducting plasma, small-scale processes dissipate magnetic energy much more rapidly than helicity $H \equiv \int \mathbf{A} \cdot \mathbf{B} \, dV$ (Taylor, 1974; Berger, 1985). With this constraint the magnetic field does not relax to a potential state, but to a linear force-free state. The gradient of oe found in this region may be indicative of this ongoing relaxation process.

2.5. *Yohkoh* SXT VS NIXT COMPARISON

In April 1993 the *Yohkoh* SXT carried out a special observing sequence simultaneous with a flight of the NIXT rocket. An inital comparison of the two datasets was carried out by Yoshida *et al.* (1995) for a quiet corona region. Because the SXT temperature response is somewhat harder than that of the NIXT (>2.5 MK for SXT vs $1–3$ MK for NIXT) it was expected that the SXT would see the hotter top portions of coronal loops while the NIXT would see the lower portions or the footpoints. This was indeed generally seen to be the case in that study.

However, subsequent evaluation of the one active region on the disk on that day is showing a completely different and unexpected result. One expects that 'all X-ray images are alike', so that the two should show toughly similar structures. Viewed from a distance, the two observations seem to be showing the same coronal features. However, detailed examination shows some remarkable discrepancies between the two.

Figure 9 shows the comparison of NIXT and *Yohkoh* SXT observations, with arrows pointing to three locations in the region. These are places where a structure or set of structures is visible in one of the images and *entirely invisible* in the other; the effect works both ways. Thus, if only one of these images were available, we would draw reonneous conclusions about the coronal structure, since there would be no indication at all that some structures are present.

The seriousness of this problem is obvious: if we intend to study the formation, stability and dynamics of coronal structures, one must first be able to see them. A partial solution to this problem is described in the next section.

3. Some Partial Solutions

The above discussion provides only a partial listing of some of the problems we are encountering in attempting to study the formation, heating, structuring and dynamics of the solar corona. In this section we describe two new instruments which will help to solve, or at least advance, some of these problem areas. The TRACE instrument will have the highest spatial resolution ever used to observe the

corona, as well as the ability to discriminate multiple temperature regimes and to view the atmosphere from the upper chromosphere up into the active region corona. The TXI is a rocket-borne payload which will have the capability of observing the entire sequence of successive ionization stages of a single element from $<10^6$ K to $>3 \times 10^6$ K, and will also determine flow velocities at these temperatures.

3.1. TRACE

The Transition Region And Coronal Explorer (TRACE) is designed to quantitatively explore the connections between fine-scale magnetic fields at the solar surface and the associated plasma structures in the solar outer atmosphere. The TRACE instrument uses multiple UV and normal-incidence XUV channels to collect images of atmospheric plasma from 10^4 K to 10^7 K. Many of the physical problems that arise in this portion of the atmosphere – plasma confinement, reconnection, wave propagation, plasma heating – arise throughout space physics and much of astrophysics as well. Although recent pogress in, e.g., numerical MHD simulations has been substantial (viz., Low, 1990), use of these models requires close guidance by the observations, because the enormous range in parameter scale sizes cannot be realized in the computations.

The telescope provides true 1 arc sec resolution (1 pixel is 0.5 arc sec) and temporal resolution as short as a fraction of a second for bright sources. Table II lists the operating spectral bands, the associated temperatures and the portions of the atmosphere covered. The instrument uses four normal incidence coatings, one for broadband UV and three for narrow band XUV operation. The UV channel includes a set of narrow-band filters at the focal plane, thereby allowing sub-channels which detect portions of the atmosphere from the photosphere to the transition region. Selection of the XUV channels is based on a thorough analysis carried out by Golub, Hartquist, and Quillen (1989), who analyzed the spectral region accessible to normal incidence techniques and determined the best lines to use for particular atmospheric features of interest.

TRACE is launched on a Pegasus-XL into a polar, Sun-synchronous orbit, thereby providing continuous observation of the Sun. Continuous observ- ing for about 8 months is planned over a 1-year baseline mission. TRACE produces data complementary with SOHO, and planning of the TRACE daily observations is being coordinated with those of SOHO.

The main components of the TRACE instrument are shown in Figure 10. The TRACE instrument consists of a 30-cm diameter Cassegrain telescope and a filter system feeding a CCD detector. Each quadrant of the telescope is coated for sensitivity to a different wavelength range. Light entering the instrument passes first through an entrance filter assembly which transmits only UV and soft X-ray radiation, thus blocking the solar heat from reaching the mirrors. A large rotating quadrant shutter selects one quadrant at a time for viewing. The secondary mirror of the telescope is active, to correct for pointing jitter to better than 0.1 arc sec.
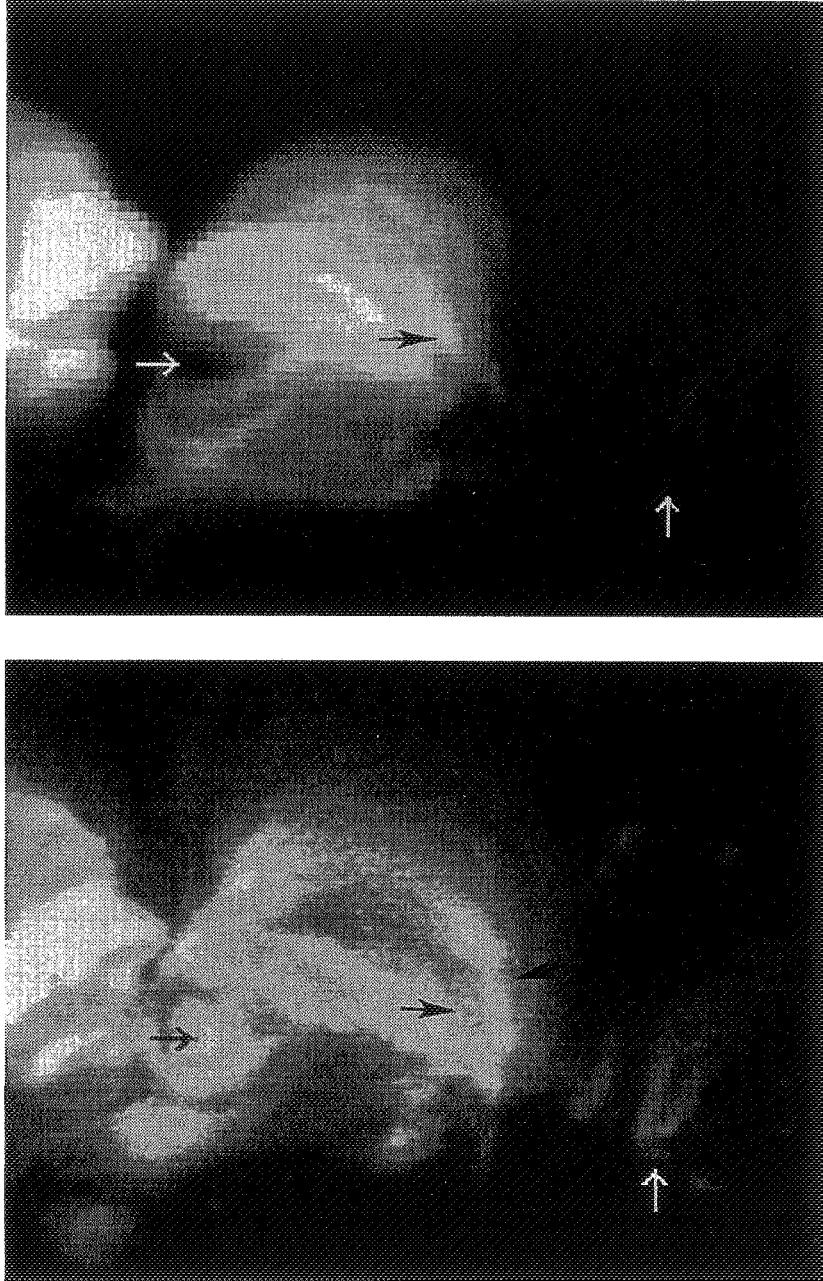
Figure 9. Comparison between *Yohkoh* (*top*) and NIXT (*bottom*) observations of an active region; arrows indicate structures seen in one of the instruments but *not* seen in the other.

Table II

TRACE spectral regions and observing parameters

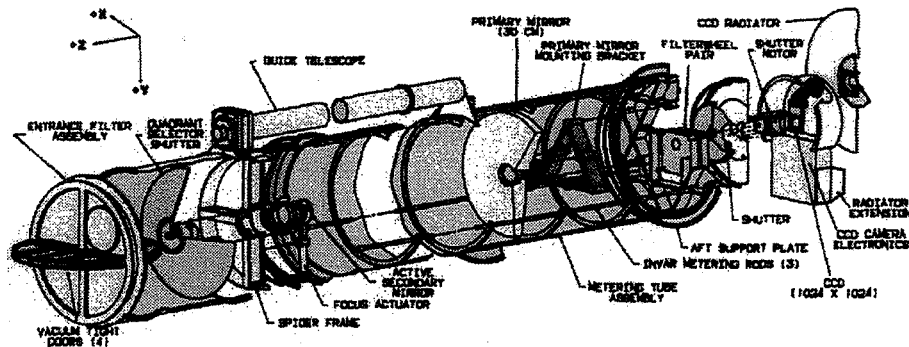| Central wavelength (Å)	Width (Å)	Ion	Location
2500	Broad	Continuum	Photosphere
1700	Broad	T_{min}/Chrom.	
1570	30	C I, Fe II, Cont.	Photosphere
1550	30	C IV	Transition region
1216	84	H Lα	Chromosphere
284	14	Fe XV	Corona
195	10	Fe XII	Corona
		(+Fe XXIV)	Flares
171	9	Fe IX	Corona

Figure 10. Major system components of the TRACE instrument.

The converging beam from the secondary mirror passes through the central hole in the primary, where it encounters two filter wheels in series, each having three filters and one open position. These wheels contain both the XUV light-blocking and the UV passband filters. Finally, there is a focal plane shutter and a $10^{24} \times 10^{24}$ CCD, for a field of view of 8.5 × 8.5 arc min. Mosaic observations are planned, for larger field and daily full disk data-taking. The TRACE launch is late in 1997, and mission lifetime is at least 8 months. Thus it will be observing during the rise phase of the new solar cycle.

Some of the scientific objectives of the mission are:

- Magnetic field structure and evolution.
- Coronal heating and magnetic fields.
- Onset of coronal mass ejections.
- Variability of X-ray bright points.

The mission and its objectives are described in more detail in Tarbell *et al.* (1994).
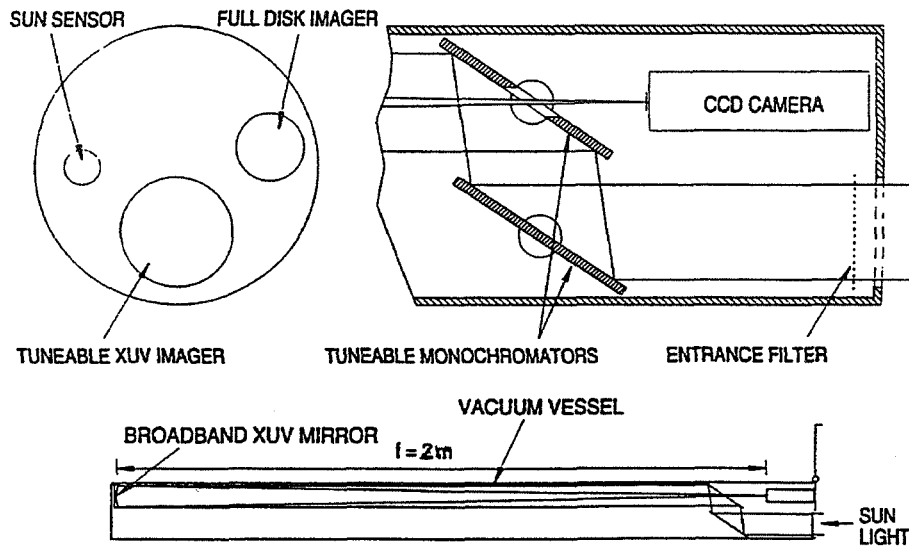
Figure 11. Schematic layout of the Tuneable XUV Imager.

3.2. TXI

The Tuneable X-ray Imager (TXI) is a high-resolution coronal imaging instrument which has the ability to produce near-monochromatic images tuneable over a range of XUV wavelengths. The present design covers the wavelength range 170–220 Å, which includes the strong series of iron lines from Fe IX through Fe XIV, inclusive. Thus, the problem of 'missing' structures is solved, for the temperature range $\log T = 5.8–6.4$, because all of the successive ionization stages are isolated and recorded.

Figure 11 shows a schematic layout of the instrument. Spectral isolation is achieved by using a double-crystal monochromator, which feeds a broadband telescope, coated with an XUV multilayer having $\Delta\lambda \sim 30$ Å (FWHM). The monochromator is made as narrow-band as possible, which in this instance is ≈ 4 Å, and it is tuned by rotating the two plane mirrors in parallel. A Cowan–Golovehenko arrangement is used (Cowan, 1983), which has the highly desireable property that the entrance and exits beams stay fixed during tuning. Thus, there is no image motion in the focal plane as the wavelength is changed.

Table III shows the strongest lines in the TXI passband. Depending upon line strength and available exposure time, it appears possible to record data out to ≈ 220 Å; no data below 170 Å are recorded because aluminum light-blocking filters are used at the entrance aperture and at the focal plane. We note that line multiplets, such as Fe XII near 193 Å, do not smear the image, because this is a non-dispersive system.

Table III
Strongest lines in the TXI passband

Ion	Wavelength (Å)	$\log T$
Fe IX	171.08	6.0
O V	172.17	5.4
O VI	172.94	5.5
	173.08	
Fe X	174.53	6.1
	177.24	
Fe XI	180.42	6.2
Si XI/Fe XII	186.88	6.2
Fe XI	188.22	6.2
Fe XXIV	192.03	7.3
Fe XII	192.40	6.2
	193.52	
	195.13	
Fe XIII	202.04	6.2
	203.82	
Fe XIV	211.32	6.3
He II	237.35	4.7

The TXI sounding rocket program has just received approval from NASA to begin construction (May 1996). Present plans are to have the payload ready to fly in two years, by the summer of 1998. A summer launch is neccessary in order to reduce absorption by the residual even at rocket altitudes. A minimum altitude of 100 miles is necessary for the wavelengths observed in this experiment, and a line-of-sight to the sun as near normal to the plane of the atmosphere as possible is required. The launch therefore takes place around local noon in White Sands, NM.

3.3. THE SOLAR RADIO TELESCOPE

Of course, it is not only in the area of space-based instrumentation that solutions to the present set of problems in solar physics may be sought. In this section we describe a representative ground-based instrument, designed to map the magnetic field structure and topology in the corona.

A proposal for a dedicated Solar Radio Telescope which represents a major advance on current radio facilities is currently being explored (a report by D. Gary and T. Bastian will be available shortly). The ability to map solar magnetic fields above coronal active regions is one of the major goals of this telescope. The features necessary to carry out such a goal are:

 — the ability to make radio images of active regions on short time scales with high spatial resolution and high dynamic range;

– the ability to make images at many closely-spaced frequencies across a broad frequency range nearly simultaneously; and

– accurate polarimetry.

The proposed instrument which provides these features consists of an array which contains many small dishes (presently planned to be 40) with full-disk coverage, three large (~25 m) dishes to provide sensitivity and allow accurate calibration, and receivers which incorporate the frequency agile characteristics so successfully demonstrated by the OVRO array with a target range from 300 MHz to 30 GHz. This instrument would have 2.5 times as many baselines as the VLA, and requires a large correlator to handle them. Recent advances in broadband microwave components, large correlators and computers make such an instrument possible for a low cost. Considerable effort will also be expended on software for real-time processing of the data into a form (images and coronal field maps) suitable for immediate use by the broader solar community.

3.3.1. *Vector Magnetic Fields*

Finally, we mention the almost obvious point that vector magnetograms are crucially important in the comparison between surface fields and coronal structure/stability. Ground-based observations have progressed enormously, but there still remains the basic question: how much of the observed variability is due to atmospheric effects and how much is intrinsic to the source? This question has been answered in part by comparing observations taken simultaneously at widely-separated sites. However, the best way to answer the question and to obtain the highest quality observations, is to place a vector magnetograph in orbit.

Acknowledgements

References

Alissandrakis, C. E.: 1981, *Astron. Astrophys.* **100**, 197.

Berger, M. A.: 1985, *Astrophys. J. Suppl.* **59**, 433.

Billings, D. E.: 1966, *A Guide to the Solar Corona*, Academic Press, New York.

Craig, I. J. D., McClymont, A. N., and Underwood, J. H.: 1978, *Astron. Astrophys.* **70**, 1.

Daw, A., DeLuca, E., and Golub, L.: 1995, *Astrophys. J.* **453**, 929.

Démoulin, P., Balala, L. G., Mandrini, C. H., Hénoux, J. C., and Rovira, M. G.: 1996, *Astron. Astrophys.*, in press.

Golub, L., Hartquist, T. W., and Quillen, A. C.: 1989, *Solar Phys.* **122**, 245.

Golub, L., Herant, M., Kalata, K., Lovas, S., Nystrom, G., Pardo, F., Spiller, E., and Wilczynski, J.: 1990, *Nature* **6269**, 842.

Gómez, D. O., Martens, P. C. H., and Golub, L.: 1993, *Astrophys. J.* **405**, 767.

Herant, M., Pardo, F., Spiller, E., and Golub, L.: 1991, *Astrophys. J.* **376**, 707.

Heyvaerts, J. and Priest, E. R.: 1984, *Astrophys. J.* **137**, 63.

Huber, M. C. E., Foukal, P. V., Noyes, R. W., Reeves, E. M., Schmahl, E. J., Timothy, J. G., Vernazza, J. E., and Withbroe, G. L.: 1974, *Astrophys. J.* **194**, L115.

Linsky, J. F. and Serio, S. (eds.): 1993, *Physics of Solar and Stellar Coronae*, Kluwer Academic Publishers, Dordrecht, Holland.

Low, B. C.: 1990, *Ann. Rev. Astron. Astrophys.* **28**, 491.

Martens, P. C. H. and Gómez, D. O.: 1992, *Publ. Astron. Soc. Japan* **44**, L187.

Metcalf, T. R., Canfield, R. C., Hudson, H. S., Mickey, D. L., Wülser, J. P., Martens, P. C., and Tsuneta, S.: 1994, *Astrophys. J.* **428**, 860.

Poletto, G., Vaiana, G. S., Zombeck, M. V., Krieger, A. S., and Timothy, A. F.: 1975, *Solar Phys.* **44**, 83.

Rosner, R., Tucker, W. H., and Vaiana, G. S.: 1978, *Astrophys. J.* **220**, 643.

Sakurai, T. and Uchida, Y.: 1977, *Solar Phys.* **52**, 397.

Sams, B. J., III, Golub, L., and Weiss, N. O.: 1993, *Astrophys. J.* **399**, 313.

Schmieder, B., Démoulin, P., Aulanier, G., and Golub, L.: 1996, *Astrophys. J.*, in press.

Shibata, K. *et al.*: 1992, *Publ. Astron. Soc. Japan* **44**, L173.

Shimizu, T., Tsuneta, S., Acton, L. W., Lemen, J. R., and Uchida, Y.: 1992, *Publ. Astron. Soc. Japan* **44**, L147.

Tarbell, T. D., Bruner, M., Jurcevich, B., Lemen, J., Strong, K., Title, A., Wolfson, J., Golub, L., and Fisher, R.: 1994, *Proc. of the 3rd SOHO Workshop*, ESA SP-373.

Taylor, J. B.: 1974, *Phys. Rev. Letters* **33**, 1139.

Uchida, Y., McAllister, A., Strong, K. T., Ogawara, Y., Shimizu, T., Matsumoto, R., and Hudson, H. S.: 1992, *Publ. Astron. Soc. Japan* **44**, L155.

Vaiana, G. S., Krieger, A. S., and Timothy, A. F.: 1973, *Solar Phys.* **32**, 81.

Yoshida, T., Tsuneta, S., Golub, L., Strong, K., and Ogawara, Y.: 1995, *Publ. Astron. Soc. Japan* **47**, L15.